sustainability

Article

Factors Influencing Post-Construction Responses of Underlying Tunnel below Excavation Base in Gravelly Clay

Sheng-Wei Xie [1,*], Yue-Hong Ye [1] and Jie Ren [2]

[1] Guangzhou Metro Design & Research Institute Co., Ltd., Guangzhou 510010, China
[2] China Construction Infrastructure Corp., Ltd., Beijing 100029, China
* Correspondence: xieshengwei@hnu.edu.cn

Abstract: This paper investigates the response mechanism behind an existing tunnel subjected to a long and deep collinear excavation in Shenzhen granite residual strata. The maximum excavation depth was 18.0 m and the minimum residual soil depth above the tunnel crown was only 6.3 m, causing appreciable tunnel heave and transverse deformation. Two-dimensional parametric numerical study is adopted to examine the impacts of influential factors (excavation dimensions, ground permeability coefficient, and exposure time of the excavation base) on the tunnel responses. The hardening soil model with small strain (HS-Small) is used to model the soil stress–strain behavior. It is found that the long-term deformation of the tunnel after excavation and unloading cannot be ignored. The soil will continue to consolidate and deform, and the tunnel will continue to heave with soil due to the dissipation of the negative excess pore water pressure. The long-term deformation of the tunnel after excavation and unloading is significantly affected by the excavation geometry. With the increase in excavation width B, the final tunnel heave after excavation and unloading increases first and then tends to be stable. Furthermore, the relative position of the tunnel and the excavation base is also one of the major contributors to the long-term deformation of the tunnel. The growth of tunnel deformation Δf and the exposure time T are exponentially negatively correlated with L_y. The change in the permeability coefficient k has no effect on the final stable tunnel heave and the growth of tunnel deformation Δf, which is exponentially negatively correlated with the exposure time T.

Keywords: displacement; excavation; long collinear; time-dependent; tunnel

check for updates

Citation: Xie, S.-W.; Ye, Y.-H.; Ren, J. Factors Influencing Post-Construction Responses of Underlying Tunnel below Excavation Base in Gravelly Clay. *Sustainability* **2022**, *14*, 11400. https://doi.org/10.3390/su141811400

Academic Editor: Suraparb Keawsawasvong

Received: 2 August 2022
Accepted: 3 September 2022
Published: 11 September 2022

1. Introduction

With the rapid development of underground transportation systems in congested urban areas, long and deep excavations are constructed for underground express roads. Excavations might be collinear with underlying existing tunnels, which can be deemed as a plane strain problem. Excavation-induced ground stress relief leads to soil heave below the excavation base. As a consequence, tunnel responses to the overlying excavation are of great concern, in terms of heave, transverse deformation, and internal forces. In unfavorable cases (e.g., poor ground conditions, deep excavation, inappropriate support stiffness, and close proximity), the existing tunnel may be severely damaged, with visible cracks and leakages [1,2], posing a great threat to the operational safety of the tunnel.

As a conventional problem, the excavation-induced tunnel responses have been extensively investigated by analytical methods [3,4], numerical methods [5–8], and centrifuge modeling [9–11]. However, well-documented case histories on behaviors of a long collinear tunnel and excavation are sparse, despite the fact that such case histories can help calibrate numerical tools and facilitate a thorough insight into the general behavior of similar scenarios. Meng et al. [11] carried out a comprehensive investigation on the tunnel responses due to overlying excavation through field observation. It was found that the development of the tunnel heave becomes more and more rapid with the increasing unloading ratio (ratio of excavation depth to tunnel cover depth). In addition, it is generally known that the tunnel responses involve complex excavation–soil–tunnel interaction mechanisms, especially in the relationship between the excavation-induced behaviors of the underlying ground (stress state change and soil heave) and the tunnel (longitudinal and transverse deformation). Furthermore, in soils with a low permeability coefficient, the excavation-induced ground and retaining system responses exhibit an appreciable time-dependent characteristic [12,13], which is majorly governed by the exposure time of the excavation base before base slab construction and the soil permeability coefficient. For instance, field observation in granite residual soil demonstrates that the average tunnel heave to reach a stable value since the end of excavation is 10.2 days [11]. However, among the earlier contributions, the responses mechanism behind the underlying existing tunnel are not well understood, and neither are the time-dependent behaviors.

To this end, this study investigates the performances of Shenzhen Metro Line 11 subjected to an overlying long and deep collinear excavation for Guimiao Road in granite residual soil. The total collinear length of the metro tunnel and the excavation is 3.1 km. Numerical analyses were carried out to interpret the response mechanisms behind the underlying tunnel. In addition, parametric study was also conducted to investigate the effects of influential factors, including geometrical dimensions, relatively position, ground permeability coefficient, and exposure time of the excavation base, on the short-term and long-term tunnel responses.

2. Problem Definition

The studied problem of this paper is a tunnel longitudinally parallel to a long excavation, which can be assumed as a plane strain problem. The system consists of the following four components: ground, diaphragm wall, base slab, and tunnel. Soil mass excavation causes stress relief and, thus, ground heave below the excavation base, which indirectly leads to additional deformations and internal forces on the underlying existing tunnel. The excavation-induced tunnel responses, principally overall heave and transverse deformation, are governed by the ground conditions (stiffness and the permeability coefficient), retaining stiffness, superstructure load, exposure time of the excavation base, and geometric variables (relative positions and dimensions). The geometric variables include the depth H, the excavation width B, and the tunnel diameter D. Differing from the rest of the parameters, the ground permeability coefficient, exposure time of the excavation base, and superstructure load only govern the long-term tunnel responses after soil mass excavation is completed. The magnitude of the surcharge of the superstructure is assumed to be the same as the greenfield soil gravity on the excavation base prior to the excavation. Due to the plastic behavior of the soil, the tunnel heave cannot be recovered after the surcharge is exerted This study aims to study the effects of the above parameters on the tunnel responses.

3. Finite Element Analysis

3.1. Engineering Background

The background for this study is a case history in Shenzhen, in which a long collinear excavation was carried out above an existing shield tunnel. The observed tunnel responses due to the overlying excavation was investigated by Meng et al. [14]. To gain a better understanding of the mechanism behind the tunnel responses subjected to the overlying excavation, an explicit numerical study on this problem was performed, focusing on the relationship between the excavation-induced arching effect below the excavation base and the tunnel deformation [15,16]. Using the aforementioned research, this study aims to use numerical simulation to figure out the influences of the major factors, including the excavation geometries, excavation-tunnel relative position, and soil permeability coefficient on the underlying tunnel deformations.

3.2. Constitutive Model and Parameters

The two-dimensional numerical analyses were carried out using the finite element program *PLAXIS-2D* [17]. Stress–strain behaviors of all structures were assumed to be linear elastic, as introduced in the previous numerical study by Meng et al. [18]. The input calculation parameters of the structures are shown in Table 1. The tunnel lining and retaining pile were modeled by 6-node plate elements. The RC strut and steel strut were modeled as a fixed-end anchor and node-to-node anchor, respectively. The stiffness of the retaining pile, base slab, and RC struts were assumed to be 80% of the nominal values. Effects of the joints on the tunnel lining stiffness in the circumference direction were considered by setting the effective stiffness ratio to be 0.7.

Table 1. Input parameters of the structures in the FE model.

Structure Type	t (m)	A (m^2)	s (m)	v	E_{red} (MPa)
Retaining pile	0.866	—	—	0.2	24,000
Steel strut	—	0.0298	3	0.2	210,000
Tunnel lining	0.35	—	—	0.2	24,150
Base slab	1.3	—	—	0.2	24,000

Abbreviations are as follows: t = thickness of plate element; A = cross sectional area; s = spacing of strut; v =Poisson's ratio; E_{red} = reduced Young's modulus, but the steel strut is a designed value.

The geological profile (see Figure 1) in the numerical model is simplified to be a uniform single layer ⑧ gravelly clay, which is the main soil encountered between the excavation base and tunnel crown in the aforementioned case history. The hardening soil model with small-strain stiffness (HS-Small model) was adopted to simulate the soil stress–strain behavior of ⑧ gravelly clay. The HSS parameters of ⑧ gravelly clay, as listed in Table 2, were determined through laboratory tests conducted by Ye (2017) [19] and validated by Meng et al. (2022) [20].

Table 2. Constitutive parameters of ⑧ gravelly clay in the FE model.

E_{50}^{ref} (kPa)	E_{ur}^{ref} (kPa)	E_{oed}^{ref} (kPa)	c' (kPa)	φ' (°)	Ψ (°)	m	v_{ur}	R_f	K_0	G_0^{ref}	$\gamma_{0.7}$
12.75	43.35	12.75	8	32	2	0.72	0.2	0.89	0.59	102.4	3.0×10^{-4}

Abbreviations are as follows: E_{50}^{ref} = reference secant stiffness of trial axial compression stress paths; E_{ur}^{ref} = reference stiffness for unloading/reloading stiffness; E_{oed}^{ref} = reference stiffness from one-dimensional compression tests; c' = effective cohesion; φ' = effective friction angle; m = power that controls the stress dependency of stiffness; Ψ = dilatancy angle; v_{ur} = Poisson's ratio of unloading/reloading; R_f = failure ratio; K_0 = at-rest earth pressure coefficient; G_0^{ref} = reference shear modulus at very small strains; and $\gamma_{0.7}$ = shear strain at which G_s = 0.722 G_0.

3.3. Geometry and Boundary Conditions

As discussed below, the maximum excavation width and depth among the parametric study is 79.6 m and 25.6 m, respectively. To avoid boundary effects, the distance between lateral boundaries and excavation peripheries was more than 120 m, nearly four times the excavation depth. Thus, the domain of all the numerical models was 300 m (width) × 80 m (height). Lateral boundaries were fixed in the horizontal direction, while the bottom boundary in both vertical and horizontal directions. The 2D FE model mesh is depicted in Figure 2.

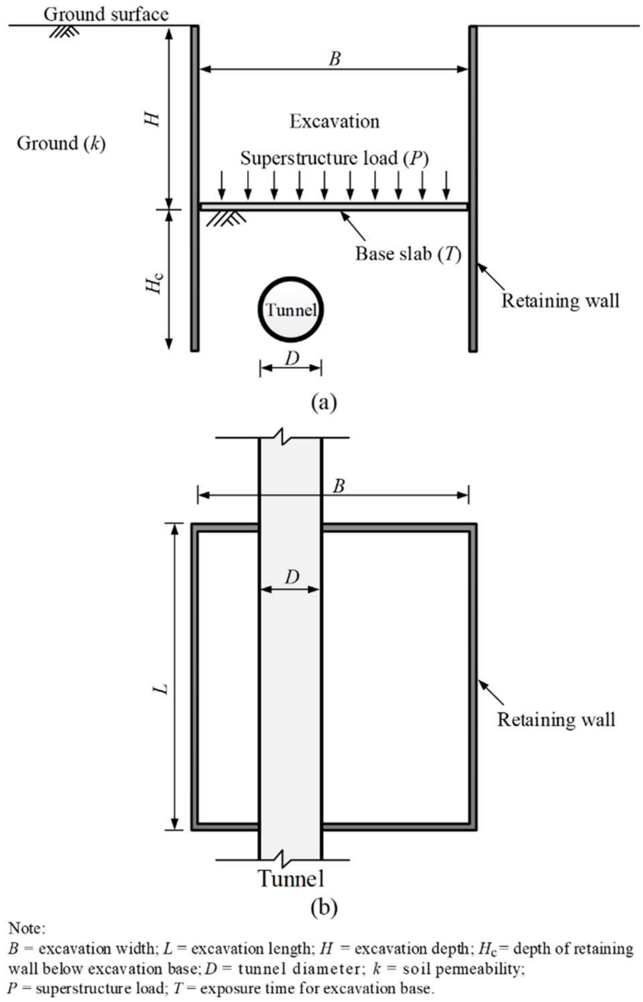

Figure 1. Problem definition: (**a**) elevation view; (**b**) plan view.

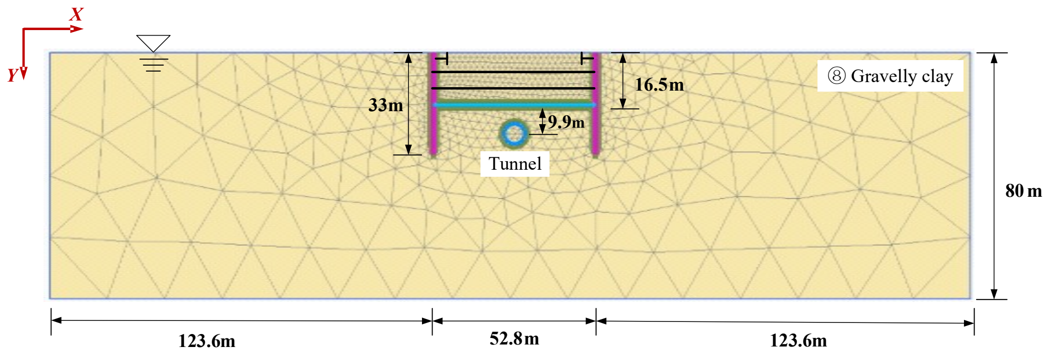

Figure 2. 2D FE mesh.

3.4. Numerical Modeling Procedure

The numerical modeling procedure was generally the same as the field condition, as follows:

(a) Phase I: initial stresses were generated in the first step using the K_0 procedure;
(b) Phase II: the tunnel structure was activated and soils within the tunnel were deactivated;
(c) Phase III: excavation procedures were simulated step-by-step as the stages listed in Table 3.

Table 3. Numerical cases.

Case	Variables					
	B/D	H/D	L_x/D	L_y/D	K (mm/day)	t (days)
0	8	2.5	0	1.5	0.001	300
B-1	4	2.5	0	1.5	0.001	300
B-2	6	2.5	0	1.5	0.001	300
B-3	10	2.5	0	1.5	0.001	300
B-4	12	2.5	0	1.5	0.001	300
H-1	8	1.5	0	1.5	0.001	300
H-2	8	2	0	1.5	0.001	300
H-3	8	3	0	1.5	0.001	300
H-4	8	4	0	1.5	0.001	300
L_x-1	8	2.5	1	1.5	0.001	300
L_x-2	8	2.5	1.5	1.5	0.001	300
L_x-3	8	2.5	2	1.5	0.001	300
L_x-4	8	2.5	3	1.5	0.001	300
L_y-1	8	2.5	0	1.2	0.001	300
L_y-2	8	2.5	0	1.8	0.001	300
L_y-3	8	2.5	0	2.5	0.001	300
L_y-4	8	2.5	0	3	0.001	300
k-1	8	2.5	0	1.5	0.0005	300
k-2	8	2.5	0	1.5	0.005	300
k-3	8	2.5	0	1.5	0.01	300
k-4	8	2.5	0	1.5	0.1	300
t-1	8	2.5	0	1.5	0.001	0.05
t-2	8	2.5	0	1.5	0.001	10
t-3	8	2.5	0	1.5	0.001	50
t-4	8	2.5	0	1.5	0.001	100

Here, L_x is the horizontal distance between the tunnel center and the base center, while L_y is the vertical distance between the tunnel center and the base.

4. Results and Discussions

The numerical model and input parameters are already validated by comparing the measured retaining pile displacement, ground surface settlement and tunnel heave, and the corresponding calculated results [12]. Hence, this study only introduces the parametric analysis results.

4.1. Excavation Width B

Cases B-1 to B-4 consider the influence of different excavation widths B on the long-term deformation of the tunnel after excavation and unloading. Here, B is $4D$, $6D$, $8D$, $10D$, and $12D$ respectively. Figure 3 depicts the upward trend of the measuring points on the top of the tunnel with time after the completion of excavation under different excavation widths B. It can be seen that the trend of the five cases is basically the same. When the excavation is completed, the tunnel heave continues to increase, and finally it tends to be stable. The increase rate of tunnel heave is fast at first, and then slow, and becomes 0 when it is stable. When B is $4D$~$12D$, the maximum tunnel heave is 31.3~43.5 mm. Within the width B, the maximum tunnel heave gradually decreases with the increase in the excavation width, and finally tends toward a stable value [21]. This is because when the B value is small, the horizontal deformation caused by the retaining piles on both sides will squeeze the tunnel and the soil around the tunnel, resulting in the increase in the tunnel heave. In the range of $4D$~$8D$, the closer the tunnel is to the retaining pile, the more obvious the squeezing effect of the retaining pile is [22]. When B is greater than $8D$, the maximum tunnel heave will not increase with the continuous increase in the width, which indicates that the tunnel has been basically not affected by the retaining pile, and that heave only occurs under the consolidation of the soil. In addition, because the influence of the overlying soil on the tunnel is limited, with the increase in B, the stress of the tunnel will not change after exceeding the influence range of the soil, and the final heave is affected by the stress, so the final stable heave will not change.

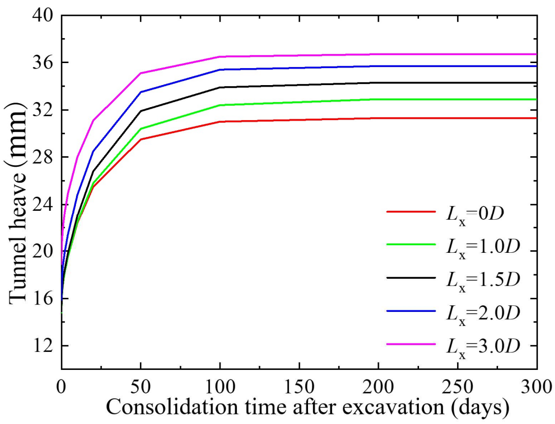

Figure 3. Development of tunnel heave after excavation is completed versus different excavation widths.

In order to describe the deformation of the tunnel due to consolidation based on the change in deformation at the completion of excavation, the parameter Δf is introduced. The larger the Δf value is, the greater the change in the tunnel due to consolidation. That is, the greater the influence of consolidation on the tunnel deformation. Here, Δf is obtained by the following Equation (1):

$$\Delta f = (f_{steady} - f_0)/f_0 \tag{1}$$

where Δf is the multiple of the increase in the tunnel heave after excavation, f_{steady} is the stability value of tunnel deformation after excavation is completed, and f_0 is the tunnel deformation when the excavation is just completed.

Figure 4 depicts the relationship between different excavation widths and Δf. It can be seen that when the excavation width B is 4D~8D, Δf shows a linear decreasing trend, and its growth rate decreases from 1.5 times to 1.1 times; however, when B is 8D~12D, Δf shows a linear increasing trend, and the increase is doubled from 1.1 to 1.33 times [23]. When the base is narrow, the increase in Δf is mainly caused by the extrusion of the retaining pile. When the excavation is wide, the tunnel has gradually moved away from the influence area of the retaining pile, and the dominant factor of Δf begins to change into the stress release caused by the unloading of the excavation.

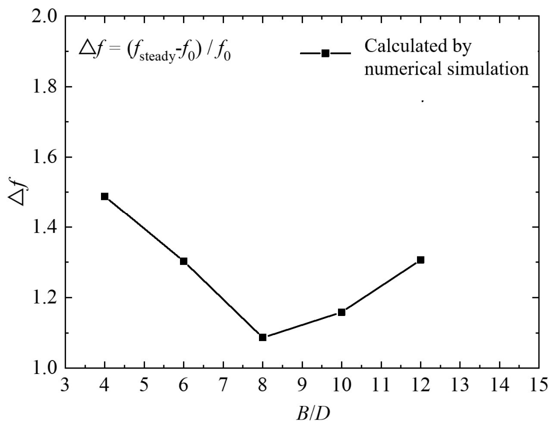

Figure 4. Variation of the increase ratio of the tunnel heave after excavation is completed versus the excavation width.

Figure 5 shows the relationship between excavation base exposure time T and excavation width B. When the ratio of the tunnel heave to the final heave reaches 95%, it is considered that the profile deformation is stable, and the corresponding exposure time is T. It can be seen from the figure that when the excavation width increases from 4D to 12D, the exposure time T gradually increases from 47 days to 93 days, that is, B is in direct proportion to T. This may be because the larger the excavation width, the more pore water pressure to there is be dissipated in the soil, so the exposure time will become longer [24].

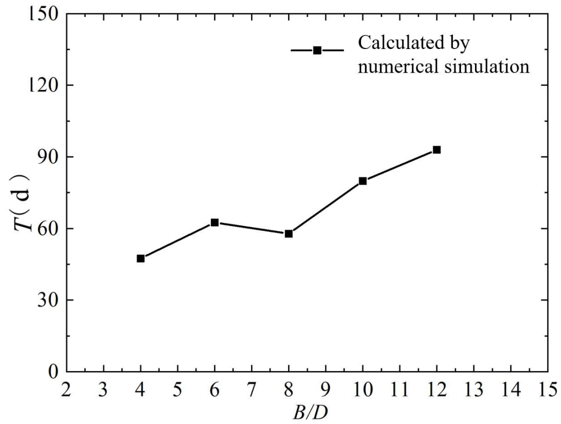

Figure 5. Variation of stable time for tunnel heave after excavation is completed versus the excavation width.

4.2. Excavation Depth H

Cases H-1 to H-4 consider the influence of different excavation depth H of the base on the long-term deformation of the tunnel after excavation and unloading. The excavation depth H is taken as 1.5D, 2D, 2.5D, 3D and 4D, respectively. Figure 6 depicts the upward trend of the measuring points on the top of the tunnel with time after the completion of excavation at different excavation depths H [25]. The results show that the trend is basically the same as in the five cases. When the excavation is completed, the tunnel heave continues to increase, and finally tends to be stable. The growth rate of tunnel heave is fast at first, and then slow, and it becomes 0 after it is stable. The excavation depth is changed from 1.5D to 4.0D, the maximum heave of the tunnel is changed from 17.2 mm to 62 mm, and the maximum deformation of the tunnel is directly proportional to the excavation depth.

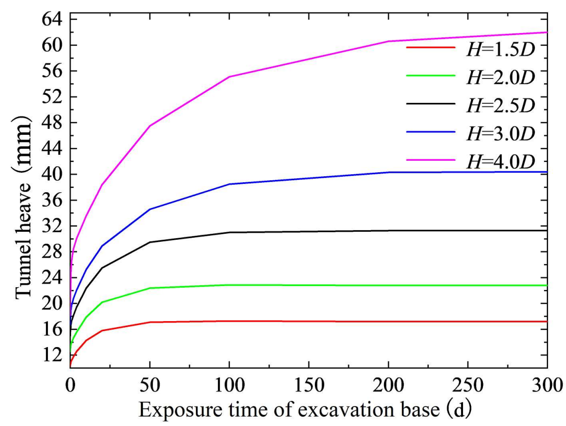

Figure 6. Development of tunnel heave after excavation is completed versus different excavation depths.

Figure 7 shows the relationship between different excavation depths H and Δf. When the excavation depth is increased from 1.5D to 4D, the increase in Δf is increased from 0.7 to 2.4 times; Δf is in direct proportion to the excavation depth. The calculation points can be well fitted with the exponential equation in origin, and the coefficient of determination R^2 is 0.997. The specific fitting equation is as follows:

$$\Delta f = 0.081 + 0.449e^{(H/D-1.069)/1.781} \tag{2}$$

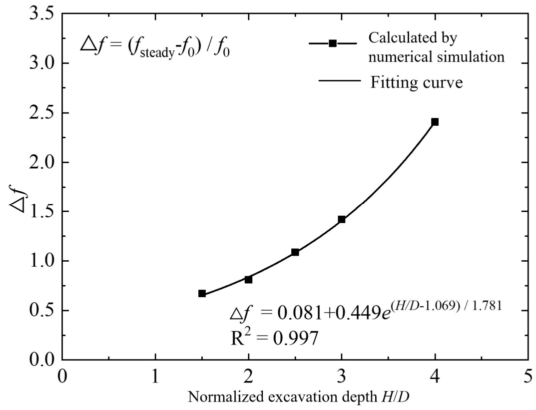

Figure 7. Variation of increase ratio of the tunnel heave after excavation is completed versus excavation depth.

Figure 8 shows the relationship between exposure time T and excavation depth H. It can be seen from the figure that when the excavation depth increases from 1.5D to 4D, the exposure time T gradually increases from 32.4 days to 169.1 days. Indeed, T is in direct proportion to the excavation depth [26]. The exponential equation can be used for better fitting. The fitting equation is a power function, and the coefficient of determination R^2 is 0.983. The specific fitting equation is as follows:

$$T = 10.46(H/D)^{2.01} \tag{3}$$

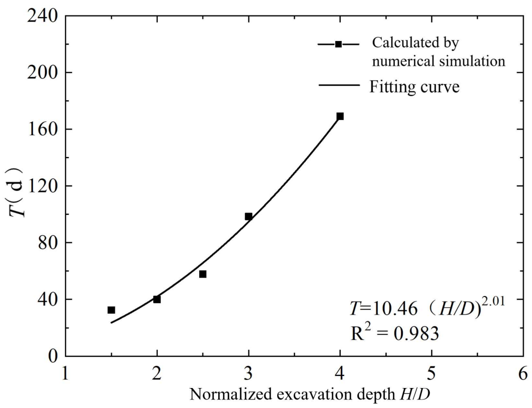

Figure 8. Variation of stable time for tunnel heave after excavation is completed versus excavation depth.

4.3. Horizontal Distance from the Excavation Center to Tunnel Center L_x

Cases L_x-1 to L_x-4 consider the influence of the horizontal distance L_x between the tunnel axis and the excavation center on the long-term deformation of the tunnel after excavation and unloading. Here, L_x is 0, 1.0D, 1.5D, 2D, and 3D respectively. Figure 9 summarizes the heave trend of the measuring points on the top of the tunnel with time after the excavation of the different horizontal distance L_x between the tunnel axis and the excavation center. The trend is basically consistent with that in Section 4.2. When L_x increases from 0D to 3D (the tunnel position changes from the excavation center to the retaining pile), the maximum tunnel heave changes from 31.3 mm to 36.7 mm, respectively. It can be seen that when the excavation width is 8D, the maximum tunnel heave gradually increases with the increase in L_x; that is, the closer the retaining pile is, the greater the maximum tunnel heave is. This is because when the tunnel is within the influence of the deformation of the retaining piles, the horizontal deformation of the retaining piles on both sides will squeeze the tunnel and the soil around the tunnel [27], resulting in the increase in the tunnel heave. This is consistent with the influence of foundation pit width on the maximum uplift of the tunnel in Section 4.1. The closer the tunnel is to the retaining pile, the more obvious the squeezing effect of the retaining pile.

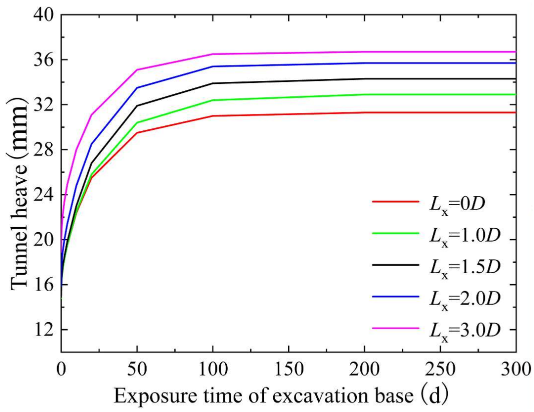

Figure 9. Development of tunnel heave after excavation is completed versus different tunnel horizontal distance from the excavation center.

Figure 10 depicts the relationship between different L_x and Δf values. It can be seen that when L_x is 0D to 1.5D, Δf shows a linear increasing trend, and the increase is increased from 1.1 to 1.3 times; when L_x is 1.5D–3D, Δf shows a linear decreasing trend, and the growth rate decreases from 1.3 times to 0.9 times. For the unloading of the excavation, it can be equivalent to the reverse uniformly distributed load applied on the excavation base surface, that is, the closer to the uniformly distributed load center, the greater the stress change caused by unloading. However, due to the influence of the extrusion effect caused by the deformation of the retaining piles around the excavation base, the deformation of the soil under the foundation pit is coupled by the change in unloading stress and the extrusion effect caused by the deformation of the retaining piles. When the tunnel is closer and closer from the center to the retaining pile (L_x = 0–1.5D), the change in horizontal position makes the squeezing effect of the retaining pile more obvious than the stress effect caused by unloading, making Δf increase. When the tunnel further approaches the retaining pile (L_x = 1.5D–3D), the stress effect caused by unloading begins to become more obvious, making Δf begin to decrease.

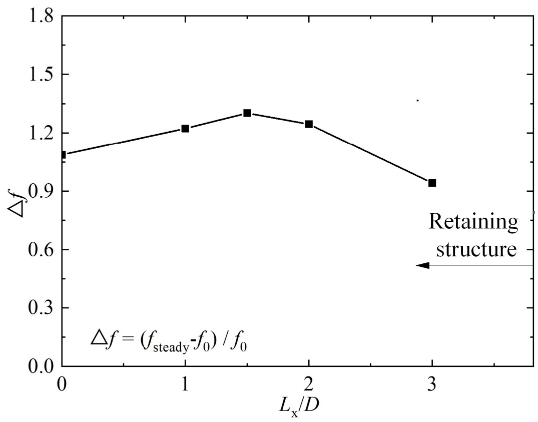

Figure 10. Variation of increase ratio of tunnel heave after excavation is completed versus tunnel horizontal distance from the excavation center.

Figure 11 shows the relationship between exposure time T and L_x. It can be seen from the figure that when L_x increases from 0D to 1D, the exposure time T gradually increases from 58 days to 71 days, and when L_x continues to increase from 1D to 3D, the exposure time T gradually decreases from 71 days to 48 days.

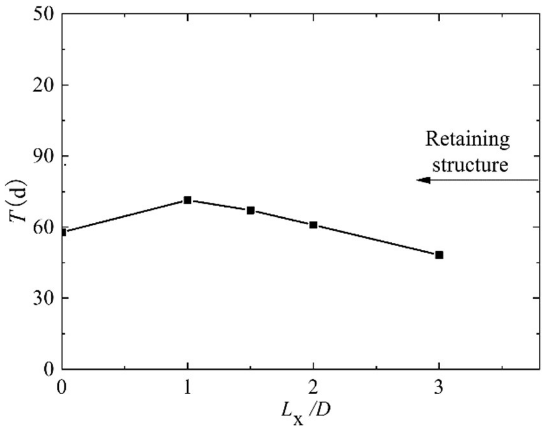

Figure 11. Variation of time of excavation completion to stabilization T and L_x.

4.4. Vertical Distance from the Excavation Base Subface to Tunnel Center L_y

Cases H-1 to H-4 consider Cases L_y-1 to L_y-4 consider the influence of the vertical distance L_y from the center of the tunnel to the excavation base on the long-term deformation of the tunnel after excavation and unloading. Here, L_y is taken as 1.2D, 1.5D, 1.8D, 2.5D, and 3D, respectively. Figure 12 summarizes the upward trend of the measuring points on the top of the tunnel with time after the excavation under the different vertical distances L_y from the tunnel axis to the excavation base. As before, the heave trend of the measuring point on the top of the tunnel of the five cases is basically the same. When L_y increases from 1.2D to 3.0D, the maximum tunnel heave decreases from 35 mm to 22 mm, and the maximum deformation value of the tunnel is inversely proportional to the excavation depth [28]. This is because the closer the tunnel is to the excavation base, the greater the stress change caused by unloading on the tunnel, resulting in a greater final tunnel heave.

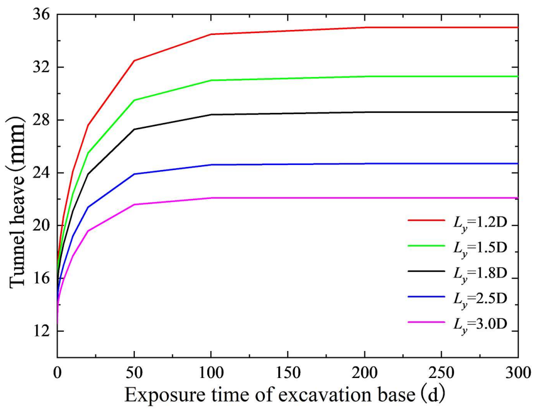

Figure 12. Development of tunnel heave after excavation is completed under different tunnel vertical distance from the excavation base.

Figure 13 shows the relationship between the vertical distance L_y from tunnel axis to the excavation base and Δf. The results show that when L_y increases from 1.2D to 3D, the growth of Δf decreases from 1.3 times to 0.75 times; Δf is inversely proportional to the excavation depth. The calculation points can be well fitted with the exponential equation, and the coefficient of determination R^2 is 0.998. The specific fitting equation is as follows:

$$T = 3.426(L_y/D)^{-0.792} \quad (4)$$

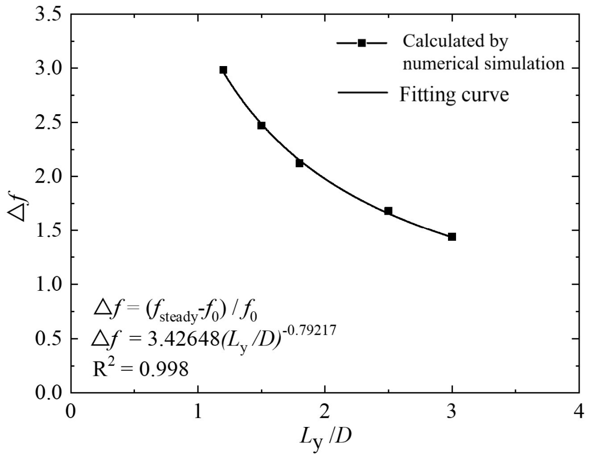

Figure 13. Variation of increase ratio of tunnel heave after excavation is completed versus the tunnel vertical distance from the excavation base.

Figure 14 depicts the relationship between the exposure time T and the vertical distance L_y from the tunnel axis to the excavation base. It can be seen from the figure that when L_y increases from 1.2D to 3D, the exposure time T gradually decreases from 68.7 days to 40.9 days. Here, T is inversely proportional to the vertical distance L_y between the tunnel axis and the excavation base. The exponential equation in origin can be used for better fitting. The fitting equation is a power function, and the coefficient of determination R^2 is 0.935. The specific fitting equation is as follows:

$$T = 74.01(L_y/D)^{-0.576} \tag{5}$$

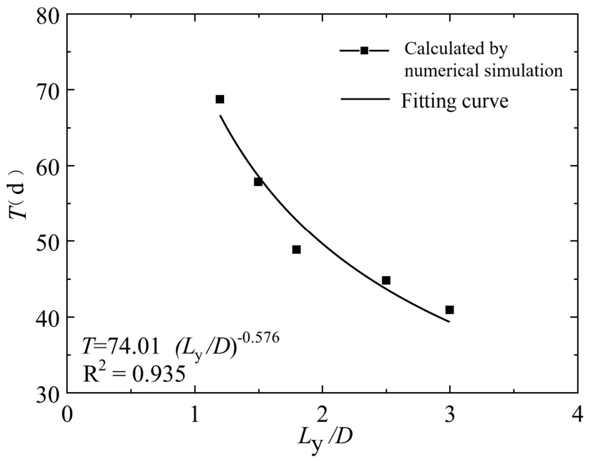

Figure 14. Variation of stable time for tunnel heave after excavation is completed with excavation depth.

4.5. Permeability Coefficient *k*

The influence of different permeability coefficient k values on the long-term deformation of the tunnel after excavation and unloading is considered in cases k-1 to k-4. The k is taken as 0.0005, 0.001, 0.005, 0.01, and 0.1 m/day, respectively. Figure 15 summarizes the upward trend of the measuring points on the top of the tunnel with time under different k. Similarly, the change trend under the five cases is basically the same. When the excavation is completed, the tunnel heave continues to increase, and finally tends to be stable [29]. The increase rate of tunnel heave is fast at first, and then slow, and it becomes 0 when it is stable. In addition, for different k, the increase rate of the tunnel heave is different. The larger the k value is, the faster the increase rate of the tunnel heave is, and the earlier it reaches the stable value, but the final tunnel heave is 31.3 mm. It can be seen that k has no effect on the final deformation value of the tunnel, but only on the heave rate of the tunnel [30]. Figure 16 depicts the relationship between the k and Δf. When k increases from 0.0005 to 0.1 m/day, the increase in Δf does not change. It can be seen that k only affects the heave rate of the tunnel after excavation and has no impact on the deformation amplitude of the tunnel and the final maximum deformation of the tunnel. The final changes in tunnel heave after the excavation is completed are governed by the excess pore water pressure generated during the excavation stage. Only the soil permeability has an impact on the speed for the changes. Hence, the normalized tunnel heave illustrated in Figure 16 is constant with varying soil permeability.

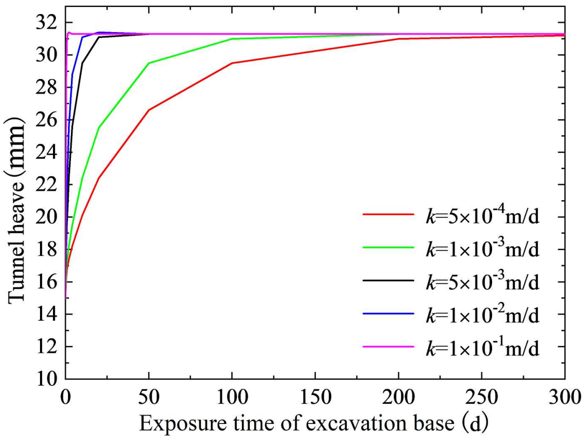

Figure 15. Development of tunnel heave after excavation is completed versus different ground permeability.

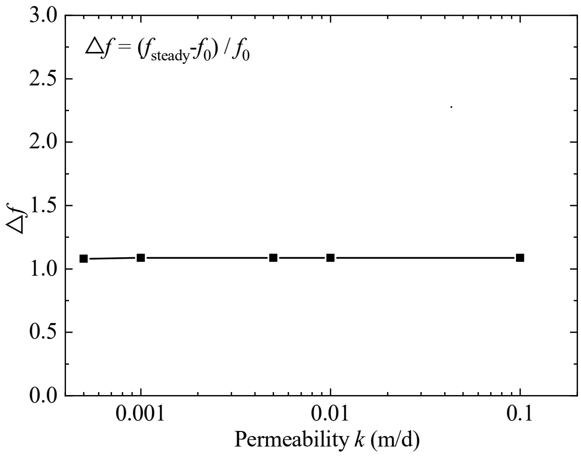

Figure 16. Variation of increase ratio of the tunnel heave after excavation is completed versus ground permeability.

Figure 17 shows the relationship between exposure time T and soil permeability coefficient k. It can be seen from the figure that when k increases from 0.0005 to 0.1 m/day, the exposure time T gradually decreases from 114 days to 0.6 days. Here, T is inversely proportional to the excavation depth. The exponential equation in origin can be used for better fitting. The fitting equation is a power function, and the coefficient of determination R^2 is 1. The specific fitting equation is as follows:

$$T = 0.06792k^{-0.97697} \quad (6)$$

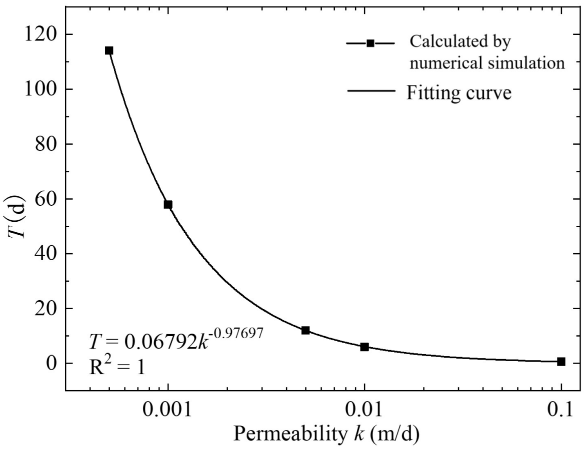

Figure 17. Variation of increase ratio of tunnel heave after excavation is completed with ground permeability.

4.6. Superstructure Construction Time t

The influence of different permeability coefficient Cases *t*-1 to *t*-4 considers the influence of different superstructure construction time t on the long-term deformation of the tunnel after excavation and unloading. The construction time t of the superstructure is taken as 0.05, 10, 50, 100, and 300 days, respectively. This because the maximum exposure time in the model is 300 days. When *t* is 300 days, it can be divided into the following two stages: before and after the construction of the superstructure. It can be seen from Figure 18 that at the moment of the construction of the superstructure, due to the influence of the instantaneous additional load, the soil skeleton produces elastic deformation, which makes the uplift deformation of the soil rapidly reduce, resulting in the rise and fall of the tunnel. Then, the tunnel consolidates and continues to heave up until the negative excess pore water pressure dissipates, and the tunnel heaves up and tends to be stable. It can be seen that the earlier the superstructure is constructed, the less the tunnel heave in the whole process can be reduced, and the more the final stable heave can be reduced. For the ideal situation that the superstructure will be constructed 0.05 days after excavation, the maximum tunnel heave is 19.8 mm. This is 27% lower than the maximum tunnel heave of 25.2 mm for when the superstructure is constructed in 300 days.

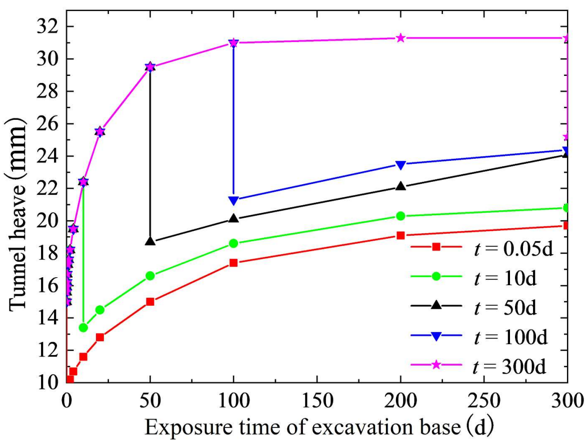

Figure 18. Development of tunnel heave after excavation is completed under different exposure times for the excavation base.

Figure 19 depicts the relationship between Δf and the construction time t of the superstructure. When t increases from 0.05 days to 50 days, the growth Δf multiplies from 0.32 to 0.61 times, Δf is positively correlated with T, and the linear fitting R^2 of this section is 0.999, as in Equation (7). When t increases from 50 days to 300 days, the growth Δf is doubled from 0.61 to 0.68 times, Δf is also linearly positively correlated with T, and the fitting R^2 is 0.994, as in Equation (8). It can be seen that the earlier the superstructure is constructed, the smaller the Δf; that is, the more obvious the inhibition effect on the upward heave of the tunnel. The later the superstructure is constructed, the more the excess pore water pressure dissipates, and the more complete the consolidation of the soil at the excavation base is, and the worse the inhibition effect is. In addition, the rate of soil consolidation is declining, so the earlier the superstructure is constructed, and the more the influence of long-term deformation of the tunnel after excavation and unloading can be reduced.

$$\Delta f = 0.3243 + 0.0057t \tag{7}$$

$$\Delta f = 0.5949 + 0.00029t \tag{8}$$

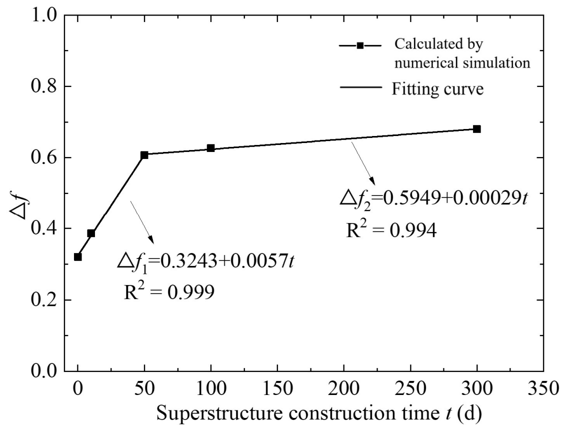

Figure 19. Variation of increase ratio of tunnel heave after excavation is completed versus the exposure time of the excavation base.

5. Conclusions

In this paper, the influence factors of long-term deformation of the underlying tunnel after excavation are analyzed by numerical simulation. The influence of the geometrical dimensions, relative position, ground permeability coefficient, and exposure time of the excavation base, on the short-term and long-term deformation of the tunnel after unloading is discussed. A series of control measures for mitigating the long-distance collinear underlying tunnel are proposed. The specific conclusions are as follows:

(1) The long-term deformation of the tunnel after excavation and unloading cannot be ignored. Due to the dissipation of the negative excess pore water pressure of the surrounding soil, the soil will continue to consolidate and deform, and the tunnel will continue to heave. With the dissipation of negative excess pore water pressure, the consolidation rate of the soil begins to decrease gradually, and the heave rate of the tunnel also decreases gradually. When the negative excess pore water pressure is completely dissipated, the soil consolidation rate drops to 0, and the tunnel heaves steadily and is basically unchanged;

(2) The long-term deformation of the tunnel after excavation is affected by the excavation size. With the increase in excavation width B, the final tunnel heave after excavation increases at first and then tends to be stable. The growth of tunnel deformation Δf decreases at first and then increases, while exposure time T gradually increases, which is basically linearly and positively correlated with the excavation width. With the increase in excavation depth H, the final tunnel heave after excavation and unloading also gradually increases. The increase in amplitude of tunnel deformation Δf is exponentially positively correlated with the excavation depth, while the exposure time T is exponentially positively correlated with the excavation depth;

(3) The long-term deformation of the tunnel after excavation and unloading is affected by the relative position of the tunnel and excavation. When the excavation width is $8D$,

with the increase in the horizontal distance L_x from the tunnel axis to the excavation center, the final stable heave value after excavation and unloading gradually increases, and the growth of tunnel deformation Δf and the exposure time T of the tunnel at first increase and then decrease. With the increase in the vertical distance L_y from the tunnel axis to the excavation base, the final stable tunnel heave after excavation and unloading gradually decreases. The growth of tunnel deformation Δf and the exposure time T are exponentially negatively correlated with L_y;

(4) The long-term deformation of the tunnel after excavation and unloading is affected by the permeability coefficient k and the exposure time T of the superstructure. The change in permeability coefficient k has no effect on the final stable tunnel heave after excavation and unloading, and the growth of tunnel deformation Δf, which is exponentially negatively correlated with the exposure time T. The earlier the superstructure is constructed, the less the tunnel heave in the whole process, and the more the final stable tunnel heave can be reduced. The relationship between the exposure time T and Δf of the superstructure is composed of two linear positive correlation functions, and the slope of the front section is greater than that of the rear section.

Author Contributions: Conceptualization, methodology, software, validation, formal analysis, investigation, resources, writing—original draft preparation, visualization, supervision, S.-W.X.; data curation, Y.-H.Y. and J.R.; writing—review and editing, review, J.R. All authors have read and agreed to the published version of the manuscript.

Funding: This study is supported by the research program of Guangzhou Metro Design & Research Institute Co., Ltd. (grant no. KY-2020-015).

Institutional Review Board Statement: Not applicable.

Informed Consent Statement: Not applicable.

Data Availability Statement: Not applicable.

Acknowledgments: Thanks to the two teachers for their guidance and help in the research architecture, experimental equipment, experimental operation, data sorting, statistical analysis, and thesis writing.

Conflicts of Interest: The authors declare no conflict of interest.

References

1. Chang, C.T.; Sun, C.W.; Duann, S.W.; Hwang, R.N. Response of a Taipei Rapid Transit System (TRTS) tunnel to adjacent excavation. *Tunn. Undergr. Space Technol.* **2001**, *16*, 151–158. [CrossRef]
2. Chen, S.L.; Lee, S.C.; Wei, Y.S. Numerical analysis of ground surface settlement induced by double-O tube shield tunneling. *J. Perform. Constr. Facil.* **2016**, *30*, 04016012-1. [CrossRef]
3. Cheng, H.Z.; Chen, R.P.; Wu, H.N.; Meng, F.Y. A simplified method for estimating the longitudinal and circumferential behaviors of the shield-driven tunnel adjacent to a braced excavation. *Comput. Geotech.* **2020**, *123*, 103595. [CrossRef]
4. Dolezalova, M. Tunnel complex unloaded by a deep excavation. *Comput. Geotech.* **2001**, *28*, 469–493. [CrossRef]
5. Sharma, J.S.; Hefny, A.M. Effect of large excavation on deformation of adjacent MRT tunnels. *Tunn. Undergr. Space Technol.* **2001**, *16*, 93–98. [CrossRef]
6. Huang, X.; Huang, H.W.; Zhang, D.M. Centrifuge modelling of deep excavation over existing tunnels. *Proc. Inst. Civ. Eng.-Geotech. Eng.* **2014**, *167*, 3–18. [CrossRef]
7. Chen, R.P.; Meng, F.Y.; Li, Z.C.; Ye, Y.H.; Ye, J.N. Investigation of response of metro tunnels due to adjacent large excavation and protective measures in soft soil. *Tunn. Undergr. Space Technol.* **2016**, *58*, 224–235. [CrossRef]
8. Tan, Y.; Wei, B. Observed behaviors of a long and deep excavation constructed by cut-and-cover technique in Shanghai soft clay. *J. Geotech. Geoenviron. Eng.* **2012**, *138*, 69–88. [CrossRef]
9. Finno, R.J.; Kim, S.; Lewis, J.; Van Winkle, N. Observed performance of a sheetpile-supported excavation in Chicago clays. *J. Geotech. Geoenviron. Eng.* **2019**, *145*, 125–129. [CrossRef]
10. Meng, F.Y.; Chen, R.P.; Kang, X.; Li, Z.C. e-p curve-based structural parameter for assessing of clayey soil structure disturbance. *Bull. Eng. Geol. Environ.* **2020**, *79*, 4387–4398. [CrossRef]
11. Meng, F.Y.; Chen, R.P.; Xie, S.W.; Wu, H.N.; Liu, Y. Observed behaviors of a long and deep excavation and collinear underlying tunnels in Shenzhen granite residual soil. *Tunn. Undergr. Space Technol.* **2020**, *103*, 103504. [CrossRef]

12. Meng, F.Y.; Chen, R.P.; Xie, S.W.; Wu, H.N.; Liu, Y.; Lin, X.T. Excavation-induced arching effect below base level and responses of long-collinear underlying existing tunnel. *Tunn. Undergr. Space Technol.* **2022**, *123*, 104417. [CrossRef]
13. Benz, T. Small-Strain Stiffness of Soils and Its Numerical Consequences. Ph.D. Thesis, University of Stuttgart, Stuttgart, Germany, 2006; p. 66.
14. Meng, F.Y.; Chen, R.P.; Xu, Y.; Wu, K.; Wu, H.N.; Liu, Y. Contributions to responses of existing tunnel subjected to nearby excavation: A review. *Tunn. Undergr. Space Technol.* **2022**, *119*, 104195. [CrossRef]
15. Ye, Y.H. Influence of Construction of Open-Cut Tunneling on Uplift Displacement of the Underneath Metro Tunnel and Its Control Measures. Master's Thesis, Zhejiang University, Hangzhou, China, 2017.
16. Clough, G.W.; O'Rourke, T.D. Construction induced movements of in-situ walls. In *Geotechnical Special Publication: Design and Performance of Earth Retaining Structures (GSP 25)*; ASCE: Reston, VA, USA, 1990; pp. 439–470.
17. Meng, F.Y.; Chen, R.P.; Kang, X. Effects of tunneling-induced soil disturbance on post-construction settlement in structured soft soils. *Tunn. Undergr. Space Technol.* **2018**, *80*, 53–63. [CrossRef]
18. Chen, R.P.; Song Xu Meng, F.Y.; Wu, H.N.; Lin, X.T. Analytical approach to predict tunneling-induced subsurface settlement in sand considering soil arching effect. *Comput. Geotech.* **2022**, *141*, 104492. [CrossRef]
19. Finno, R.J.; Atmatzidis, D.K.; Perkins, S.B. Observed performance of a deep excavation in clay. *J. Geotech. Eng.* **1989**, *115*, 1045–1064. [CrossRef]
20. Lo, K.Y.; Ramsay, J.A. The effect of construction on existing subway tunnels-a case study from Toronto. *Tunn. Undergr. Space Technol.* **1991**, *6*, 287–297. [CrossRef]
21. Finno, R.J.; Roboski, J.F. Three-dimensional responses of a tied-back excavation through clay. *J. Geotech. Geoenviron. Eng.* **2005**, *131*, 273–282. [CrossRef]
22. Peck, R.B. Deep excavation and tunneling in soft ground. State-of-the-art-report. In Proceedings of the 7th International Conference of Soil Mechanics and Foundation Engineering, International Society of Soil Mechanics and Geotechnical Engineering (ISSMGE), Mexico City, Mexico, 29 August 1969; pp. 225–281.
23. Tan, Y.; Wang, D.L. Characteristics of a large-scale deep foundation pit excavated by the central-island technique in Shanghai soft clay. I: Bottom-up construction of the central cylindrical shaft. *J. Geotech. Geoenviron. Eng.* **2013**, *139*, 1875–1893. [CrossRef]
24. O'Rourke, T.D. Ground movements caused by braced excavations. *J. Geotech. Eng. Div.* **1981**, *107*, 1159–1178. [CrossRef]
25. Cheng, Z.K.; Wang, D.G.; Ding, Y.C.; Hang, J.Z.; Gu, Q.; Wang, J.H. Analysis of Waterfront Excavation Adjacent to Pile-supported Wharves. *New Front. Eng. Geol. Environ.* **2013**, *9*, 53–56.
26. Ge, X.W. Response of a Shield-Driven Tunnel to Deep Excavations in Soft Clay. Ph.D. Thesis, The Hong Kong University of Science and Technology, Hong Kong, China, 2002.
27. Ou, C.Y.; Liao, J.T.; Lin, H.D. Performance of diaphragm wall constructed using the top-down method. *J. Geotech. Geoenviron. Eng.* **1998**, *124*, 798–808. [CrossRef]
28. Hsieh, P.G.; Ou, C.Y. Shape of ground surface settlement profiles caused by excavation. *Can. Geotech. J.* **1998**, *35*, 1004–1017. [CrossRef]
29. Leung, E.H.Y.; Ng, C.W.W. Wall and ground movements associated with deep excavations supported by cast in situ wall in mixed ground conditions. *J. Geotech. Geoenviron. Eng.* **2007**, *133*, 129–143. [CrossRef]
30. Mindlin, R.D. Forces at a point in the interior of a semiinfinite solid. *J. Appl. Phys.* **1936**, *7*, 195–202.